

Topological polarization and surface flat band in insulators

T. T. Heikkilä¹ and G.E. Volovik^{2,3}

¹*Department of Physics and Nanoscience Center, University of Jyväskylä,
P.O. Box 35 (YFL), FI-40014 University of Jyväskylä, Finland*

²*Low Temperature Laboratory, Aalto University, P.O. Box 15100, FI-00076 Aalto, Finland*

³*Landau Institute for Theoretical Physics, acad. Semyonov av., 1a, 142432, Chernogolovka, Russia*
(Dated: December 22, 2024)

Tetrads of elasticity are a relevant tool for studying three dimensional topological insulators. These tetrads produce three elastic $U(1)$ gauge fields \mathbf{E}_μ^a , which together with the electromagnetic $U(1)$ gauge field A_μ enter the mixed topological Chern-Simons terms in the action. We consider two classes of insulators, with the topological action correspondingly $\int E^a \wedge A \wedge dA$ and $e_{abc} \int E^b \wedge E^c \wedge dA$, with $a = 1, 2, 3$. They describe the 3D intrinsic quantum Hall effect and topological polarization, respectively. The response of the current and polarization to deformations is quantized in terms of integer topological quantum numbers, N_a and N^a correspondingly. These invariants are dual to each other, being determined as integrals over dual manifolds in the reciprocal space. For a simple Hamiltonian, the insulators of the second class have flat bands on their boundaries. These flat bands give rise to the quantized polarization in the topological insulators of this class. The boundary flat bands, which are extended to the whole surface Brillouin zone, have the largest possible density of states. This suggests that the topological insulators of the second class may be included in the competition whose final goal is room-temperature superconductivity.

PACS numbers:

I. INTRODUCTION

Elasticity tetrads is a convenient way to discuss non-linear elastic deformations in terms of curved space.¹ On the other hand, they have the dimension of inverse length, which is different from the dimensionless conventional tetrads in general relativity. These tetrads provide a proper description of different topological phenomena in topological insulators,^{2,3} and they can be extended to the relativistic quantum fields and gravity.⁴

One of such topological phenomena described in terms of elasticity tetrads is the electric polarization, which is an interesting phenomenon by itself, see e.g. Refs. 5–8. Being expressed via the elasticity tetrads, the corresponding action in topological insulators contains a dimensionless prefactor representing topological polarization.³ This is different from the topological charge showing up in the quantum Hall effect, see Fig. 1.

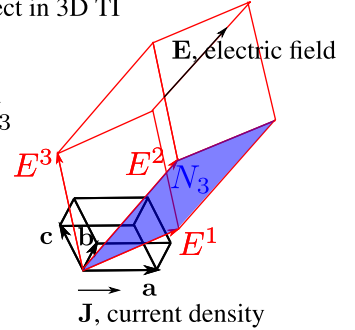
The topology determining the exotic polarization is also responsible for the formation of an (approximate) flat band on the surface of nodal line semimetals,^{9–12} nodal line superconductors¹³ superfluids,¹⁴ and topological insulators.¹⁵

Here we discuss the topological polarization and flat band using an extension of a simple model⁹ to a different range of parameters. In this extension the multiple Dirac points in a quasi 2D system evolve into a flat band, which occupies the whole 2D Brillouin zone (BZ) on the boundaries of the 3D system when the number of atomic layers increases. This is accompanied by the formation of a topological insulator state in the bulk. We consider the topological action in the bulk in terms of elasticity tetrads and the corresponding topological invariants responsible for the flat band and calculate an exotic polar-

Quantum Hall effect in 3D TI

$$\sigma = \frac{dJ}{dE}$$

$$\frac{d\sigma}{dE^3} = \frac{e^2}{2\pi h} N_3$$



Quantized polarization jump in 3D TI

$$\frac{dP}{dS^{12}} = \frac{1}{8\pi^2} N^3$$

$$S^{12} = \mathbf{E}^1 \times \mathbf{E}^2 \cdot \hat{c}$$

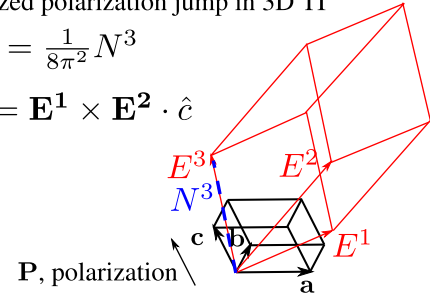


FIG. 1: Elementary cells of a crystal in real (spanned by \mathbf{a} , \mathbf{b} , \mathbf{c}) and reciprocal spaces (E^a). Quantum Hall effect¹⁶ is determined by the topological charge N_a integrated over the surface spanned by a pair of E^a , whereas the polarization jump is described by the charge N^a integrated along one E^a .

ization caused by the flat bands.

II. TOPOLOGICAL POLARIZATION IN 3+1 INSULATORS

A. Elasticity tetrads

Let us consider the theory of crystal elasticity using the approach of Refs. 1,2. The deformed crystal structure can be described as a system of three crystallographic surfaces of constant phase $X^a(x) = 2\pi n^a$, $n^a \in Z$ with $a = 1, 2, 3$. The intersection of the surfaces

$$X^1(\mathbf{r}, t) = 2\pi n^1, \quad X^2(\mathbf{r}, t) = 2\pi n^2, \quad X^3(\mathbf{r}, t) = 2\pi n^3, \quad (1)$$

are the nodes of a deformed crystal lattice. The elasticity tetrads are gradients of the phase functions:

$$E_i^a(x) = \partial_i X^a(x). \quad (2)$$

In an equilibrium crystal lattice the quantities E_μ^a are lattice vectors of the reciprocal Bravais lattice. In a deformed crystal, but in the absence of dislocations the tetrads E_μ^a satisfy the integrability condition

$$\nabla_\nu E_\mu^a - \nabla_\mu E_\nu^a = 0. \quad (3)$$

Being gradients of dimensionless functions X^a , these tetrads have dimension of inverse length, $[E_\mu^a] = 1/[l]$. This is the main difference to the dimensionless tetrads used in the theories of general relativity. However, in some theories the gravitational tetrads also have dimension $1/[l]$, see Refs. 17–21.

Moreover, due to periodicity of the crystal, the functions X^a play the role of $U(1)$ fields, and thus the tetrads play the role of the vector potentials of the effective gauge fields. This is why they can be used in the construction of new topological terms alongside with the $U(1)$ electromagnetic field. The new terms contain a mixture of the electromagnetic A_μ and elastic E_μ^a gauge fields.

B. Anomalous QHE in 3D topological insulators

In particular, the elasticity tetrads are important for a proper description of the intrinsic (without external magnetic field) quantum Hall effect in 3D topological insulators.¹⁶ The corresponding topological action (the Chern-Simons topological term), which is responsible for this effect, contains the elasticity tetrad as a dynamical gauge field in addition to the electromagnetic gauge field:²

$$S[A, A, E] = \frac{1}{4\pi^2} \sum_{a=1}^3 N_a \int d^4x E_\mu^a \epsilon^{\mu\nu\alpha\beta} A_\nu \partial_\alpha A_\beta. \quad (4)$$

Since this action is topological, the prefactor is expressed in terms of the topological quantum numbers. There are three integer coefficients N_a , which are expressed in

terms of integrals of the Green's functions in the energy-momentum space:

$$N_a = \frac{1}{8\pi^2} \epsilon_{ijk} \int_{-\infty}^{\infty} d\omega \int dS_a^i \text{Tr}[(G_\omega G^{-1})(G_{p_j} G^{-1})(G_{p_k} G^{-1})]. \quad (5)$$

Here $G_\omega \equiv \partial G / \partial \omega$, $G_{p_i} \equiv \partial G / \partial p_i$, the momentum integral is over the 2D torus — the 2D boundary \mathbf{S}_a of the elementary cell of the 3D reciprocal lattice, see Fig. 1.

For a simple orthorhombic lattice, the topological charge describing the QHE in, say, the (x, y) -plane is N_z . It is the integral in the (p_x, p_y) plane of the elementary cell of the reciprocal lattice at fixed p_z (in insulators the integral does not depend on p_z):

$$N_z = \frac{1}{4\pi^2} \int_{-\infty}^{\infty} d\omega \int dp_x dp_y \text{Tr}[(G_\omega G^{-1})(G_{p_x} G^{-1})(G_{p_y} G^{-1})]. \quad (6)$$

While in 2D crystals the topological invariant describes the quantization of the Hall conductance, the topological invariants N_a in 3D crystals describe the quantized response of the Hall conductivity to deformation:

$$\frac{d\sigma_{ij}}{dE_k^a} = \frac{e^2}{2\pi h} \epsilon_{ijk} N_a. \quad (7)$$

The presence of the reciprocal lattice vector E_k^a of dimension $1/[l]$ leads to a proper dimension of the 3D conductivity.

C. Flat bands in 3D topological insulators

Three topological invariants N_a , which are responsible for the 3D QHE, are expressed in terms of the integrals over three cross sections of the elementary cell of the three-dimensional reciprocal lattice. The other class of topological invariants represents the three invariants N^a expressed in terms of integrals over a line along the vector of the reciprocal Bravais lattice as in Fig. 1. Such a line forms a closed loop, which may accumulate a Zak phase π , see e.g. Refs. 9,10.

The invariants N^a can be considered as dual to the three invariants N_a . For example, while the invariant N_3 is an integral over the surface formed by two vectors, $\mathbf{E}^1 \wedge \mathbf{E}^2$, the invariant N^3 is an integral on the path along the vector \mathbf{E}^3 . There is also the topological invariant based on all three vectors of the reciprocal lattice: it is expressed in terms of the integral over the whole volume of the elementary cell in the reciprocal space, $\mathbf{E}^1 \wedge \mathbf{E}^2 \wedge \mathbf{E}^3$. Examples of such topological invariant are provided by the superfluid ³He-B and Standard Model of particle physics,²² when they are considered on the lattice.

In some cases the invariants N^a can be written in terms of an effective Hamiltonian $H(\mathbf{p}) = 1/G(\mathbf{p}, \omega = 0)$, which is the inverse of the Green's functions at zero frequency.

Here we assume that the insulator is PT symmetric, i.e. obeys the combination of time reversal and space inversion symmetries, and thus the PT operation commutes with the Hamiltonian. It is important that the operator PT is local in momentum space (see also^{23,24}), so that we can write the invariant in terms of an effective Hamiltonian. In particular, for an orthorhombic lattice the invariant is

$$N^z(p_x, p_y) = \frac{1}{2\pi i} \text{Tr} \left[PT \oint dp_z H^{-1} \nabla_{p_z} H \right]. \quad (8)$$

Similar to the invariant $N_z(p_z)$, which does not depend on p_z in insulators, the invariant $N^z(p_x, p_y)$ does not depend on the transverse momenta \mathbf{p}_\perp in the gapped systems (insulators or superconductors).

In noninteracting PT -symmetric insulators these invariants determine the Berry phase change along the loop (Zak phase), which is πN^a . In nodal line semimetals the nonzero Zak phase produces zero-energy surface states, which form a flat band^{9,10}. In the insulators, where the invariants do not depend on p_\perp , the flat band occupies the whole Brillouin zone on the corresponding boundaries of the sample. Note that the exact flatness of these surface bands rely on a chiral symmetry often present especially in nodal line superconductors¹³, but also in approximative descriptions of nodal line semimetals.⁹ This symmetry is not necessary for the stability of the nodal lines^{12,15}, but in its absence the surface states become "drumhead" states with some dispersion.

D. Anomalous polarization in 3D topological insulators

The dual invariants N^a are applied to the topological action that can be considered dual to the action (4), where one gauge field A_μ is substituted by the tetrad gauge field.³ The 3D topological polarization is described by the following topological term for the topological insulator:

$$S[A, E, E] = \frac{1}{16\pi^2} \sum_{a=1}^3 N^a e_{abc} \int d^4x E_\mu^b E_\nu^c e^{\mu\nu\alpha\beta} \nabla_\alpha A_\beta. \quad (9)$$

Since the term (9) is linear in the electric field $\mathcal{E} = \partial_t \mathbf{A} - \nabla A_0$, three invariants N^a ($a = 1, 2, 3$) characterize the topological polarization $\delta S[A, E, E]/\delta \mathcal{E}$ along three directions.

Let us consider for simplicity an orthorhombic crystal with an electric field along z . Then the appropriate part of the action contains the invariant N^3 :

$$S[A, E, E] = \frac{N^3}{8\pi^2} \int d^4x (\mathbf{E}^1 \times \mathbf{E}^2) \cdot \mathcal{E} = \frac{N^3}{8\pi^2} \int d^4x \mathbf{S}^{12} \cdot \mathcal{E}, \quad (10)$$

where \mathbf{S}^{12} is the area of the 2D BZ in the plane perpendicular to the normal of the considered boundary.

Electric polarization is determined as the response of the action to the electric field \mathcal{E} in the limit of zero electric field, $\mathcal{E} \rightarrow 0$. From Eq. (10) it looks that for the topological insulator with $N^a \neq 0$, the polarization is nonzero in zero electric field, which is however forbidden by parity symmetry, or by the PT invariance. In fact, it is forbidden for the infinite sample, while in the presence of boundaries this is possible, since boundaries violate parity symmetry. In the presence of two boundaries there are two degenerate ground states with opposite polarization. In one state the positive electric charges are concentrated on the upper boundary (with electric charge $+|e|/2$ per one state in the flat band), and the negative charges are on the lower boundary. In the other degenerate state the polarization is opposite. The first state is obtained as a response to the electric field $\mathcal{E}_z \rightarrow +0$, while the second state is obtained in the limit $\mathcal{E}_z \rightarrow -0$. This means that the topological polarization can be considered as the difference in polarization, when the electric field changes sign.

Recent calculations of the topological polarization in nodal loop semimetals have been done in Ref. 7. We consider this for those topological insulators where the quantization takes place. Similar to the response of the QHE to deformations in Eq. (7), which is quantized in topological insulators in terms of invariants N_a , the response of the topological polarization to the proper strains is quantized in terms of the invariants N^a . From Eq. (10) it follows that the proper strain is the deformation of the cross section area in the reciprocal lattice:

$$\frac{dP^i}{dS^{ab,k}} = \frac{1}{8\pi^2} \delta_k^i e_{abc} N^c. \quad (11)$$

For the simple orthorhombic crystal and for polarization along z one has:

$$\frac{dP^z}{dS^{12}} = \frac{1}{8\pi^2} N^3. \quad (12)$$

This derivative of the polarization with respect to deformation is an example of the well defined "differential" polarization^{5,6}. Note that the polarization itself is not quantized, but its derivative with respect to deformation in Eq. (11) is quantized.

III. ANOMALOUS POLARIZATION AND FLAT BAND

In 3D topological insulators, the same invariant N^a hence determines both the flat band on the surface of the materials and the topological polarization. The reason for that is that at each \mathbf{p}_\perp the system represents a 1+1 topological insulator, and thus for each \mathbf{p}_\perp there should be a zero energy state on the boundary. Thus for the topological insulators with nonzero N^c the flat band exists on the surface for all \mathbf{p}_\perp . This is distinct from nodal line semimetals, where the region of the surface flat band is bounded by the projection of the nodal line

to the boundary. The topological insulator phase can be obtained when the Dirac loop is moved to the boundary of the BZ.

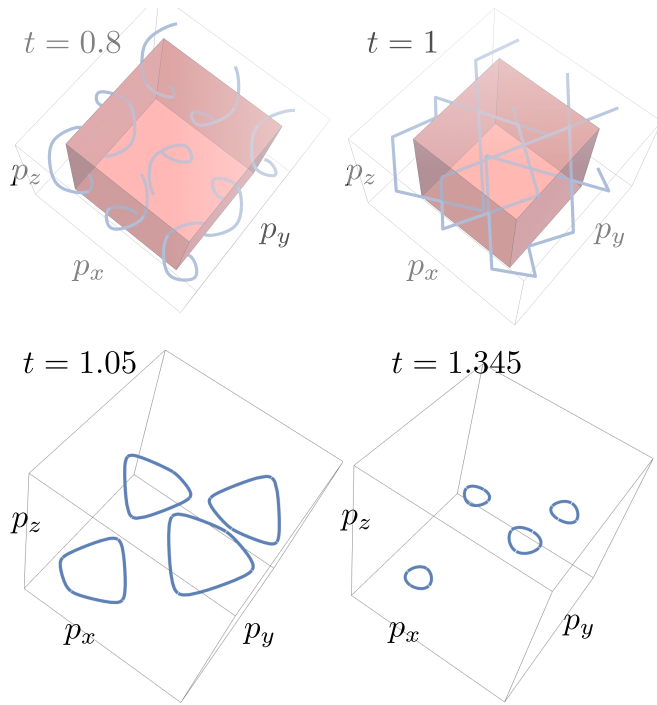


FIG. 2: Nodal lines for different parameters t . In top figures showing the spiral lines up to $t = 1$, the first Brillouin zone is shown as a box. In bottom figures, only the first Brillouin zone is plotted.

This can be checked using an extension of the model in Ref. 9 with $f = \sin p_x + i \sin p_y - t e^{-i a p_z}$, i.e. the Hamiltonian in the limit of infinite number of layers is

$$H = \sigma_x (\sin p_x - t \cos(a p_z)) + \sigma_y (\sin p_y - t \sin(a p_z)). \quad (13)$$

For low enough t , the nodal line can be found at the momenta p_x, p_y, p_z that simultaneously nullify the coefficients of $\sigma_{x,y}$. This model has three different phases depending on the value of the coefficient t as illustrated in Figs. 2 and 3. For $t < 1$, the first Brillouin zone contains four spiral lines, one inside it, others going through the Brillouin zone boundaries. In this case there are surface flat bands at the projection of the spirals to the surfaces. At $t = 1$ these lines touch and cut each other to form closed nodal line loops when $1 < t < \sqrt{2}$. The projection of these loops to the surface still mark the boundaries of the surface flat bands. Finally, for $t = \sqrt{2}$ the loops shrink into four nodal points and vanish for $t > \sqrt{2}$ in which case the system forms a topological insulator. In this case the flat band extends throughout the 2D Brillouin zone of the transverse momenta. This behavior is qualitatively similar to that found for the slightly more complicated model of rhombohedrally stacked honeycomb lattice.¹⁵

The topological invariant is in Eq. (5) of Ref. 9, where the PT operator is played by σ_z . In terms of the Green's

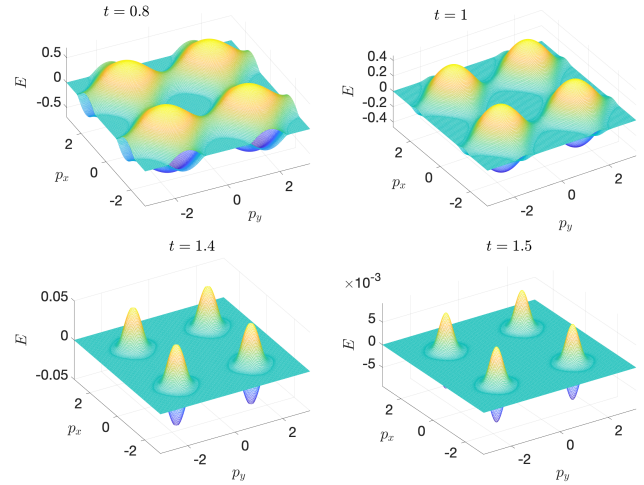


FIG. 3: Two lowest-energy eigenstates near $E = 0$, showing how for $t < \sqrt{2}$ the flat bands extend through part of the first Brillouin zone, and for $t > \sqrt{2}$ across the entire B.Z. In the figure with $t = 1.5$, the shown finite energy is associated to the finite number of layers in the simulation (note the energy scale that is lower than in other plots). All plots are computed with $N = 51$ layers.

function the invariant is in Eq. (8) of Ref. 9:

$$N^3(\mathbf{p}_\perp) = \frac{1}{4\pi} \oint_{-\pi/a}^{\pi/a} dp_z \int_{-\infty}^{\infty} d\omega \hat{\mathbf{g}} \cdot \left(\frac{\partial \hat{\mathbf{g}}}{\partial p_z} \times \frac{\partial \hat{\mathbf{g}}}{\partial \omega} \right), \quad (14)$$

which is $N^z(\mathbf{p}_\perp) = 1$ for Hamiltonian in Eq. (13).

For a finite number of layers the Hamiltonian matrix is

$$H_{ij} = (\sigma_x \sin p_x + \sigma_y \sin p_y) \delta_{ij} - t (\sigma^+ \delta_{i,j+1} + \sigma^- \delta_{i,j-1}). \quad (15)$$

This can be used to compute the spectrum shown in Fig. 3. Moreover, using the (spinor) eigenstates $\phi_n(j, p_x, p_y)$ of the finite-system Hamiltonian corresponding to eigenenergy ϵ_n , we also get the charge density at layer j

$$\rho_j = \rho_0 - e \sum_n \int_{BZ} \frac{d^{(2)}p}{(2\pi)^2} f(\epsilon_n) \phi_n(j, p_x, p_y)^\dagger \phi_n(j, p_x, p_y). \quad (16)$$

Here the integral goes over the 2D Brillouin zone of size S^{12} of the transverse momenta, $f(\epsilon)$ is the Fermi function and $\rho_0 = e S^{12} / (4\pi^2)$ ensures a charge neutral situation at zero chemical potential. We calculate everything at at zero temperature.

In a given electric field, the polarization can be computed as

$$P^z = \frac{1}{2} \sum_{j=1}^N \rho_j \text{sgn}(j - N/2), \quad (17)$$

We calculate this polarization in the case of an applied electric field similarly as in Ref. 7 (see Appendix for

details).²⁵ We mostly concentrate on the case of negligible screening, i.e., disregard the back-action of the charge density to the electric field. This corresponds to the limit $\alpha \rightarrow 0$ in Ref. 7. The results are shown in Fig. 4. Due to the presence of the flat bands, a small electric field leads to a charge density that is antisymmetric with respect to the center of the system (the average charge hence vanishes), i.e., a non-zero charge polarization. This polarization jumps rather abruptly as a function of the sign of the electric field. The size of the jump is

$$P^z(\mathcal{E}_z > 0) - P^z(\mathcal{E}_z < 0) = e \frac{\Omega_{\text{FB}}}{4\pi^2}, \quad (18)$$

where Ω_{FB} is the area of the flat band in momentum space. In the topological insulator phase $t > \sqrt{2}$ the size of the flat band becomes equal to the size of the 2D Brillouin zone, $\Omega_{\text{FB}} = S^{12}$, and hence we get the result of Eq. (12).

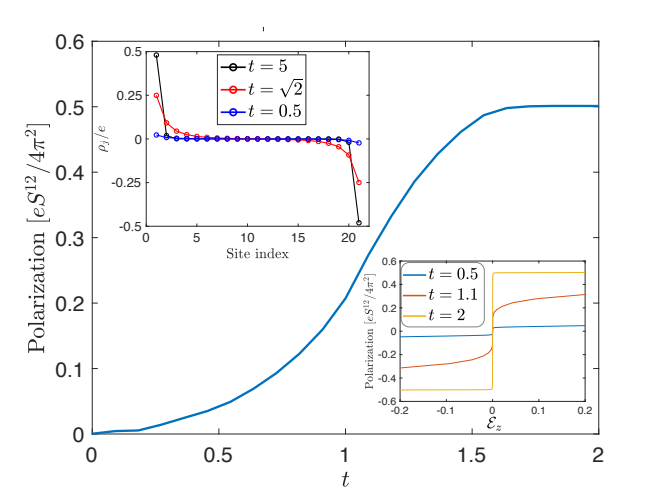


FIG. 4: Polarization as a function of the hopping parameter t driving two Lifshitz transitions from two types of nodal line semimetals at $t < 1$ and $1 < t < \sqrt{2}$ to a topological insulator phase at $t > \sqrt{2}$. Upper inset: charge density for a few parameter values indicated in the legend. Lower inset: polarization as a function of the electric field \mathcal{E}_z . If not specified otherwise, the figures are calculated with $N = 21$ layers, and with electric field $\mathcal{E}_z = 0.1$.

Note that the model described here contains a chiral symmetry: H anticommutes with the PT symmetry operator σ_z . Such chiral symmetries are typically not encountered in crystal lattices, but they may be approximate symmetries in their model Hamiltonians (for the case of rhombohedral graphite, see Ref. 28). Chiral symmetry breaking terms do not destroy the surface states, but in their presence the surface states become drum-head states with a non-zero bandwidth $\delta\epsilon$. In this case the polarization no longer contains an abrupt jump as a function of the field, but the jump has a finite width. Nevertheless, its size remains the same as in Eq. (18).

IV. CONCLUSION

The topological invariant (Zak phase) in Eqs. (8) and (14) describes two phenomena: the topological response of polarization to the strain and the flat band. This demonstrates that the topological polarization comes from the filling of the zero energy surface states. We found that the response of the polarization to the properly defined deformations is quantized, see Eq. (11). This is distinct from the nodal line semimetals, where there is also a flat band. But this flat band occupies only part of the surface BZ, and as a result there is no quantization. The derivative with respect to the deformation becomes quantized when the nodal line is moved to the boundaries of the BZ and annihilate forming a topological insulator.

This situation is very similar to that in the intrinsic 3D QHE. In the 3D topological insulators it is the derivative of the Hall conductivity which is quantized². In the Weyl semimetals such quantization is absent, but is restored when the Weyl nodes move to the boundaries of the BZ and annihilate forming a topological insulator.

Systems with flat bands are strongly susceptible to interaction induced broken symmetry phases such as superconductivity.¹¹ There, the (mean field) transition temperature T_c is proportional to the volume of the flat band, if the flat band is formed in the bulk,²⁷ or to the area of the flat band if it is formed on the surface of nodal line semimetals, and thus they may have a higher T_c . This means that topological insulators may be included in the competition whose final goal is room-temperature superconductivity.

This work has been supported by the European Research Council (ERC) under the European Union's Horizon 2020 research and innovation programme (Grant Agreement No. 694248) and the Academy of Finland (project No. 317118).

Appendix A: Appendix: details of the numerics

Figure 2 is produced by a parametric plot exhibiting the simultaneous solutions to the equations

$$\sin(p_x) = t \sin(p_z); \sin(p_y) = t \cos(p_z).$$

Figure 3 is obtained by constructing the $2N \times 2N$ matrix corresponding to Eq. (15). The plotted quantity corresponds to the two center eigenvalues, which are the lowest-energy eigenstates at $\mu = 0$ for the particle-hole symmetric Hamiltonian.

Figure 4 finds the eigenstates of the Hamiltonian $H_{ij} - \mu_j \delta_{ij}$ with a layer dependent potential μ_j . To mimic an electric field in the direction perpendicular to the layers, we follow Ref. 7 and choose

$$\mu_j = \mathcal{E}_z(j - N/2).$$

Using the resulting eigenstates and -energies, we then calculate the charge density Eq. (16) and polarization Eq. (17). Note that this approach neglects the changes into μ_j that would come from solving the Poisson equation. It hence corresponds to the limit $\kappa \rightarrow \infty$ or $\alpha \rightarrow 0$ in Ref. 7. The case of a finite κ would lead to a possibility of broadening of the polarization step, but would

not affect the size of the step. Moreover, we have studied the effects of chiral symmetry breaking terms (that do not anticommute with σ_z). They lead to a non-vanishing bandwidth of the surface states similar to what happens in rhombohedral graphite²⁸. As long as such terms are weak, they only broaden the polarization jump but do not change its overall magnitude.

-
- ¹ I.E. Dzyaloshinskii, and G.E. Volovick, Poisson brackets in condensed matter, *Ann. Phys.* **125** 67–97 (1980).
- ² J. Nissinen and G.E. Volovik, Elasticity tetrads, mixed axial-gravitational anomalies, and (3+1)-d quantum Hall effect, *Phys. Rev. Research* **1**, 023007 (2019), arXiv:1812.03175.
- ³ Xue-Yang Song, Yin-Chen He, Ashvin Vishwanath, and Chong Wang, Electric polarization as a nonquantized topological response and boundary Luttinger theorem, arXiv:1909.08637.
- ⁴ G.E. Volovik, Dimensionless physics, arXiv:2006.16821.
- ⁵ R. Resta, Macroscopic polarization in crystalline dielectrics: the geometric phase approach, *Rev. Mod. Phys.* **66**, 899 (1994).
- ⁶ R. Resta, Electrical polarization and orbital magnetization: the modern theories, *J. Phys.: Condens. Matter* **22**, 123201 (2010).
- ⁷ Y. Ominato, A. Yamakage and K. Nomura, Electric polarization in magnetic topological nodal semimetal thin films, *Condens. Matter* **3**, 43 (2018).
- ⁸ N.P. Armitage and Liang Wu, On the matter of topological insulators as magnetoelectric, *SciPost Phys.* **6**, 046 (2019)
- ⁹ T.T. Heikkilä and G.E. Volovik, Dimensional crossover in topological matter: Evolution of the multiple Dirac point in the layered system to the flat band on the surface, *Pis'ma ZhETF* **93**, 63–68 (2011); *JETP Lett.* **93**, 59–65 (2011); arXiv:1011.4185.
- ¹⁰ T.T. Heikkilä, N.B. Kopnin and G.E. Volovik, Flat bands in topological media, *Pis'ma ZhETF* **94**, 252–258 (2011); *JETP Lett.* **94**, 233–239 (2011); arXiv:1012.0905.
- ¹¹ N.B. Kopnin, T.T. Heikkilä and G.E. Volovik, High-temperature surface superconductivity in topological flat-band systems, *Phys. Rev. B* **83**, 220503(R) (2011); arXiv:1103.2033.
- ¹² A.A. Burkov, M.D. Hook and L. Balents, Topological nodal semimetals, *Phys. Rev. B* **84**, 235126 (2011).
- ¹³ A.P. Schnyder and Shinsei Ryu, Topological phases and surface flat bands in superconductors without inversion symmetry, *Phys. Rev. B* **84**, 060504(R) (2011).
- ¹⁴ V.B. Eltsov, T. Kamppinen, J. Rysti, G.E. Volovik, Topological nodal line in superfluid ³He and the Anderson theorem, arXiv:1908.01645.
- ¹⁵ T. Hyart, R. Ojajarvi, T. T. Heikkilä, Two topologically distinct Dirac-line semimetal phases and topological phase transitions in rhombohedrally stacked honeycomb lattices, *J. Low Temp. Phys.* **191**, 35–48 (2018).
- ¹⁶ Here the invariant N_3 describes a system with a broken time reversal symmetry, in which case the quantum Hall effect is an anomalous Hall effect. The spin quantum Hall effect without time reversal breaking can be obtained by a simple modification of the invariant to include the PT symmetry operator inside the trace.
- ¹⁷ D. Diakonov, Towards lattice-regularized Quantum Gravity, arXiv:1109.0091.
- ¹⁸ A.A. Vladimirov and D. Diakonov, Phase transitions in spinor quantum gravity on a lattice, *Phys. Rev. D* **86**, 104019 (2012).
- ¹⁹ Y.N. Obukhov and F.W. Hehl, Extended Einstein-Cartan theory a la Diakonov: The field equations, *Phys. Lett. B* **713**, 321–325 (2012).
- ²⁰ A.A. Vladimirov and D. Diakonov, Diffeomorphism-invariant lattice actions, *Physics of Particles and Nuclei* **45**, 800 (2014).
- ²¹ G.E. Volovik, Dimensionless physics, submitted to *JETP*, arXiv:2006.16821.
- ²² G.E. Volovik, Topological invariants for Standard Model: from semi-metal to topological insulator, *Pis'ma ZhETF* **91**, 61–67 (2010); *JETP Lett.* **91**, 55–61 (2010); arXiv:0912.0502.
- ²³ Y.X. Zhao, A.P. Schnyder and Z.D. Wang, Unified theory of PT and CP invariant topological metals and nodal superconductors, *Phys. Rev. Lett.* **116**, 156402 (2016).
- ²⁴ C.-K. Chiu, Y.-H. Chan and A.P. Schnyder, Quantized Berry phase and surface states under reflection symmetry or space-time inversion symmetry, arXiv:1810.04094.
- ²⁵ The codes needed to reproduce Figs. 3 and 4 will be linked to a published work.
- ²⁶ Cheng-Cheng Liu, Chen Lu, Li-Da Zhang, Xianxin Wu, Chen Fang, and Fan Yang, Intrinsic topological superconductivity with exactly flat surface bands in the quasi-one-dimensional $A_2Cr_3As_3$ (A=Na, K, Rb, Cs) superconductors, *Phys. Rev. Research* **2**, 033050 (2020).
- ²⁷ V.A. Khodel and V.R. Shaginyan, Superfluidity in system with fermion condensate, *JETP Lett.* **51**, 553 (1990).
- ²⁸ N.B. Kopnin, M. Ijäs, A. Harju, and T.T. Heikkilä, *Phys. Rev. B* **87**, 140503 (2013).